Nanoscale

PAPER

View Article Online
View Journal | View Issue

Cite this: *Nanoscale*, 2017, **9**, 12032

Novel inorganic perovskite quantum dots for photocatalysis†

Ge Gao,[a,b] Qiaoyue Xi,[a,c] Hua Zhou,[a] Yongxia Zhao,[a] Cunqi Wu,[a] Lidan Wang,[a]* Pengran Guo*[d] and Jingwei Xu*[a]

Received 20th June 2017,
Accepted 25th July 2017

DOI: 10.1039/c7nr04421f

rsc.li/nanoscale

Herein, we report the performance of $CsPbX_3$ (X = Cl, Br, and I) perovskite quantum dots (QDs) for photocatalytic degradation of organic dyes. The photocatalytic performance of $CsPbX_3$ QDs was characterized by UV-vis absorption spectra and ESI-MS, which evaluated their ability of degrading methyl orange (MO) solution under visible light irradiation. Interestingly, both $CsPbCl_3$ and $CsPbBr_3$ QDs show excellent photocatalytic activities, which can decompose the MO solution into a colorless solution within 100 min. This study demonstrates the potential of $CsPbX_3$ QDs in the degradation of organic dyes and environmentally friendly applications. Moreover, the integration of $CsPbX_3$ QDs and photocatalysis provides a new insight for the design of new photocatalysts.

Introduction

In recent years, industrial emission of organic dyes has become one of the main sources of environmental pollution. Due to the toxicity, the organic dyes pose a serious threat to human health.[1,2] Thus, the conversion of organic dyes into harmless substances is essential for human life and sustainable development. Solar energy, the clean and renewable energy, shows great potential in addressing environmental problems. The utilization of solar energy for environmental remediation is being extensively studied worldwide.[3–9] Among various solar energy conversion technologies, photocatalysis has been proven to be an efficient and promising way of resolving the aforementioned issues.[10] During the past several decades, much effort has been devoted to developing low cost, stable, and efficient photocatalysts, which can work especially under visible light. To date, a variety of photocatalysts, mainly including metal oxides, metal sulfides, and metal (oxy) nitrides (TiO_2,[11] ZnO,[12] SnO_2,[13] CdS,[14] and PbS[15]), have been reported. However, at a given visible light wavelength, the utilization of solar energy is far below the solar radiation energy reaching the earth. Considering the huge potential of solar + catalyst → clean environment, photocatalysis has been considered as a crucial part of chemistry and material fields. Moreover, it is highly essential to develop new photocatalysts, particularly those that can harvest the full range of visible light photons, to enhance the solar conversion efficiency.[16]

Among the large variety of photocatalyst materials, perovskite can serve as a promising photocatalyst because of its efficient photocatalytic performance, structural simplicity, and flexibility. The ideal perovskite has a cubic structure with a chemical formula of ABX_3, where A and B are cations and X is an anion. The cation A can be either organic or inorganic, for example, methylammonium (MA^+, organic cation) and Cs^+ (inorganic cation). B is a divalent metal ion, such as Pb^{2+}, and X is a halogen element (Cl^-, Br^-, or I^-). To date, about two hundred perovskite photocatalysts have been reported. Recently, a new semiconductor nanomaterial, an all-inorganic halide perovskite QD system, $CsPbX_3$, was reported by Kovalenko group and Li group.[17,18] $CsPbX_3$ with a perovskite crystal structure is a type of important optoelectronic materials. It has been the subject of intense study due to its many dramatic properties including excellent stability,[19] ultra-high photoluminescence quantum yield, absorption spectra covering the entire visible range,[17,20] size-tunable band gap,[21] and versatile chemical processability.[22] It has found application in photovoltaic, laser, third-generation solar cell, and light-emitting diode devices.[23,24] Sun and co-workers reported quantum dot light emission based on all-inorganic perovskite $CsPbBr_3$, showing a maximum luminance of 3853 cd m^{-2}, with a current density of ≈8.89 cd A^{-1} and an external quantum efficiency of ≈2.21.[25] Luther reported α-$CsPbI_3$ QD films as the active component of efficient optoelectronic devices, showing an open-circuit voltage of 1.23 V and an

[a]*State Key Laboratory of Electroanalytical Chemistry, Changchun Institute of Applied Chemistry, Chinese Academy of Science, Changchun, Jilin, 130022, China. E-mail: wangld@ciac.ac.cn, jwxu@ciac.ac.cn*
[b]*University of Science and Technology of China, Hefei, Anhui, 230026, China*
[c]*University of Chinese Academy of Sciences, Beijing, 100049, China*
[d]*Guangdong Provincial Key Laboratory of Emergency Test for Dangerous Chemicals, Guangdong Institute of Analysis, Guangzhou, 510070, China. E-mail: prguo@fenxi.com.cn*

†Electronic supplementary information (ESI) available: Additional of XRD and EDX images of the catalysts. See DOI: 10.1039/c7nr04421f

efficiency of 10.77%.[26] In such a short time, $CsPbX_3$ QDs system has shown better performance in many fields. However, to date, no study has been reported on the photocatalytic performance of $CsPbX_3$ QDs.

In this study, we provide an initial report on the important and practical property of all-inorganic perovskites for the photocatalytic decomposition of MO. First, the $CsPbX_3$ QDs are prepared by an emulsion and demulsion method at room temperature. Then, the as-prepared $CsPbX_3$ QDs are added to the MO solution. It has been found that the $CsPbCl_3$ and $CsPbBr_3$ QDs exhibit excellent photocatalytic activities, which can decompose the MO solution into a colorless solution within 100 min. The simple synthetic method, superior photocatalytic performance, large-scale synthesis, and less energy consumption for future real application make them excellent photocatalysts. Due to their photocatalytic activities, the all-inorganic perovskites may provide new photocatalysts for the decomposition of organic pollutants; moreover, this study may promote further investigations on all-inorganic perovskites to obtain a new insight into the field of photocatalysis.

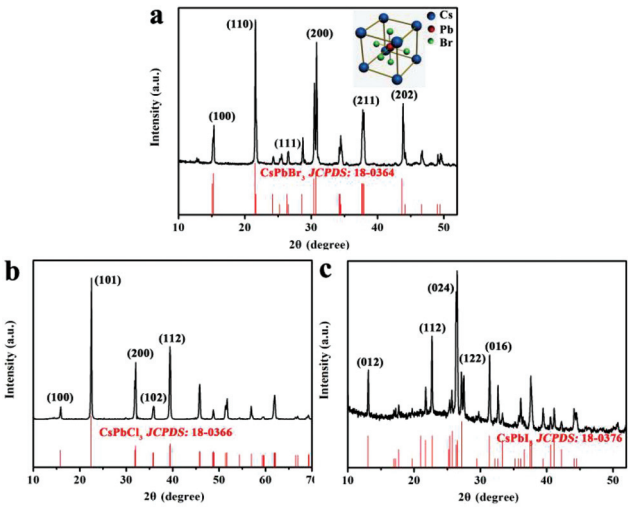

Fig. 1 The XRD patterns of the $CsPbX_3$ QDs: (a) $CsPbBr_3$, (b) $CsPbCl_3$, and (c) $CsPbI_3$. The inset of (a) shows the atomic crystal structure of $CsPbBr_3$.

Results and discussion

Synthesis of $CsPbX_3$ QDs at room temperature

The synthesis processes of the $CsPbX_3$ QDs are as follows: emulsion fabrication and demulsion.[27] First, CsX and PbX_2 (X = Cl, Br, and I) are dissolved in dimethyl sulfoxide (DMSO). Then, oleic acid (OA) and oleylamine (OAm) are added as surface ligands. In this experiment, DMSO is used as the aqueous phase, and OA and OAm are used as surfactants to stabilize the QDs. The carboxyl and amine groups in OA and OAm are adsorbed on the surface of the QDs during the reaction, and the surface alkyl group promotes the dispersion of QDs in different organic media. Finally, the abovementioned solution is quickly added to toluene under vigorous stirring. The products are obtained *via* centrifugation and further cleaned using an ethanol/toluene mixture.

Structure and composition analysis

The crystal textures of $CsPbX_3$ QDs were characterized *via* XRD profiles. The XRD image of $CsPbBr_3$ is shown in Fig. 1a. The strong and sharp peaks revealed that the $CsPbBr_3$ QDs are highly crystallized and exhibit a single-phase perovskite structure. The monoclinic perovskite structure model of $CsPbBr_3$ QDs is shown in the inset of Fig. 1a. The peaks at 2θ = 15.2, 21.5, 26.3, 30.7, 37.6, and 43.7° correspond to the diffractions from {100}, {110}, {111}, {200}, {211}, and {202} crystal planes of $CsPbBr_3$. The XRD pattern demonstrates that all the XRD peaks are consistent with monoclinic $CsPbBr_3$ (JCPDS no. 18-0364), and no characteristic impurity peaks are observed; this implies high purity of the $CsPbBr_3$ products.

The diffraction peaks of $CsPbCl_3$ and $CsPbI_3$ are shown in Fig. 1b and c, which correspond to the tetragonal and orthorhombic perovskite structures, respectively. All these results confirm the formation of $CsPbX_3$ QDs. Moreover, the XRD data of $CsPbCl_3$, $CsPbBr_3$, and $CsPbI_3$ after degradation experiments are shown in Fig. S1.† The EDX spectra (Fig. S2†) are used for chemical analysis of the QDs, which indicate that Cs, Pb, and X are the total elemental components without any other impurities.

Morphology and nanostructure analysis

The morphology and nanostructure of $CsPbX_3$ QDs are further investigated *via* transmission electron microscopy (TEM) and high-resolution transmission electron microscopy (HRTEM). As shown in Fig. 2a and b, the sphere-like $CsPbCl_3$ QDs are highly dispersed with an ultrasmall size; the averaged diameter is 3.5 nm (Fig. 2d). The HRTEM image of a single $CsPbCl_3$ QD shows well-resolved lattice fringes with a spacing of 0.28 nm (Fig. 2c), corresponding to the (002) lattice planes of the tetragonal perovskite structure of $CsPbCl_3$ QDs. Moreover, the fast Fourier transform (FFT) pattern reveals the multiple crystalline structure with {002}, {102}, and {301} facets; this is in agreement with the wide-angle XRD pattern. Fig. S3a–e† shows the TEM images, size distribution, and FFT pattern of the $CsPbBr_3$ QDs. The $CsPbBr_3$ QDs show a polyhedral structure with an average size of 8.5 nm (Fig. S3d†), which is much larger than that of the $CsPbCl_3$ QDs. The HRTEM image reveals that the lattice fringes are coherently extended across the whole nanoparticle, indicating good crystallization of $CsPbBr_3$ QDs. Moreover, the FFT pattern illustrates the lattice fringes with the space distances of 0.29 nm, which can be attributed to the (002) planes of monoclinic $CsPbBr_3$. As shown in Fig. S3f–j,† the orthorhombic perovskite structure of $CsPbI_3$ QDs has a well-defined morphology and lattice fringes as well, and the average size is about 9.0 nm. In general, the abovementioned analysis confirms the formation of $CsPbX_3$ QDs with a uniform size, unambiguous morphology, and high crystal quality.

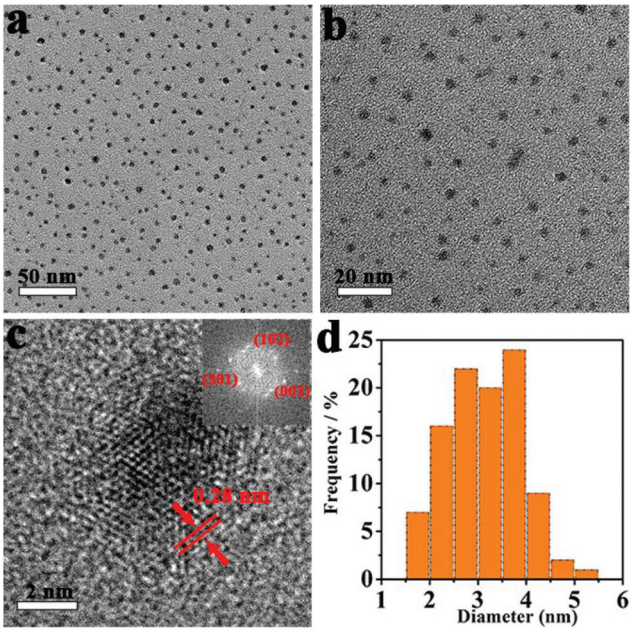

Fig. 2 (a)–(c) TEM and HRTEM images of $CsPbCl_3$ QDs. (d) Size distribution of $CsPbCl_3$ QDs. The inset of (c) shows the FFT image of the $CsPbCl_3$ QDs.

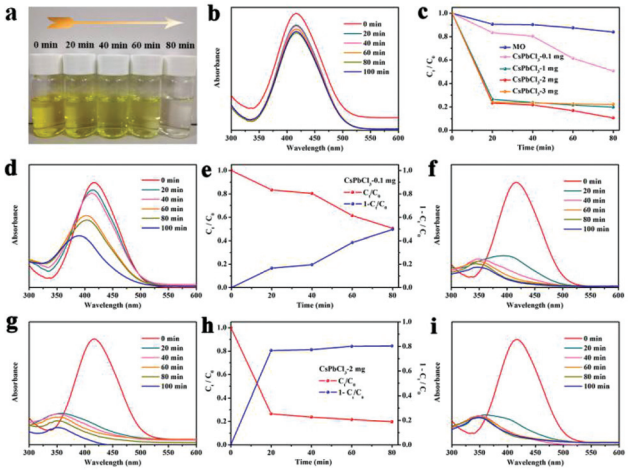

Fig. 3 (a) Image of MO degradation using $CsPbCl_3$ QDs. (b) The UV-vis spectra of MO degradation in the absence of catalysts. (c) Concentration (C_t/C_0) changes of MO with different catalysts under visible light irradiation. (d), (f), (g), and (i) show the UV-vis spectra of MO degradation using $CsPbCl_3$-0.1 mg, $CsPbCl_3$-1 mg, $CsPbCl_3$-2 mg, and $CsPbCl_3$-3 mg, respectively. Changes in the MO degradation efficiency ($1 - C_t/C_0$) using (e) $CsPbCl_3$-0.1 mg and (h) $CsPbCl_3$-2 mg.

Photocatalytic activity

The photocatalytic activity of $CsPbX_3$ QDs was investigated *via* the degradation of MO, a common organic pollutant.[28,29] $CsPbX_3$ QDs were added in various amounts: 0.1 mg, 0.5 mg, 1 mg, 1.5 mg, 2 mg, and 3 mg. These samples were designated as $CsPbX_3$-0.1 mg, $CsPbX_3$-0.5 mg, $CsPbX_3$-1 mg, $CsPbX_3$-1.5 mg, $CsPbX_3$-2 mg, and $CsPbX_3$-3 mg. The time-dependent UV-vis absorption spectra of MO under light irradiation with $CsPbCl_3$-0.1 mg, $CsPbCl_3$-1 mg, $CsPbCl_3$-2 mg, and $CsPbCl_3$-3 mg as catalysts are presented in Fig. 3d, f, g, and i, respectively. The intensity of the absorption peak was gradually diminished and blue-shifted as the irradiation time increased from 0 to 80 min. The blue shift can be attributed to dealkylation.[30] Under visible light irradiation, only 17% of MO is decomposed after 80 min in the absence of the catalyst (Fig. 3b and c). The photocatalytic activity presents a manifest increase (about 50% MO degradation in 80 min) when $CsPbCl_3$-0.1 mg is used as the catalyst. The photocatalytic activity continues to increase with the increase in the content (1 mg and 2 mg) of $CsPbCl_3$. The $CsPbCl_3$-1 mg can decompose 80% MO in 80 min. More significantly, $CsPbCl_3$-2 mg can decompose 90% MO in 80 min. However, with a further increase in the content of $CsPbCl_3$ to 3 mg, the photocatalytic activity decreases and the photodegradation time increases, as shown in Fig. 3c and i.

The time-dependent UV-vis absorption spectra of MO with $CsPbBr_3$-0.1 mg, $CsPbBr_3$-0.5 mg, $CsPbBr_3$-1 mg, and $CsPbBr_3$-1.5 mg as catalysts are presented in Fig. S4.† Under visible light irradiation, only 12% of MO was decomposed after 100 min in the absence of catalysts. The photocatalytic activity presents an obvious increase (about 55% MO degradation in 100 min) when $CsPbBr_3$-0.1 mg is used as a catalyst. The photocatalytic activity continues to increase with an increase in the content of $CsPbBr_3$ from 0.5 mg to 1 mg. The $CsPbBr_3$-1 mg can decompose about 89% MO in 100 min. However, upon a further increase in the content of $CsPbBr_3$ to 1.5 mg, the photocatalytic activity decreases, as shown in Fig. S4a and e.†

Fig. S4f† shows the UV-vis absorption spectra with $CsPbI_3$-2 mg as a catalyst. Under visible light irradiation, the catalyst exhibits a certain degree of catalytic activity before 80 min. However, the photocatalytic activity does not increase with the prolongation of irradiation time. This is because the stability of the $CsPbI_3$ sample is poor, and this sample will be decomposed after exposure to air for a certain period of time. In addition, the XRD patterns of the catalyst after degradation experiments confirm the degradation of the $CsPbI_3$ QDs (Fig. S1†).

Fig. 3c and S4a† exhibit the concentration (C_t/C_0) changes of MO with different catalysts. The photodegradation efficiency is not apparent in the absence of catalysts. The same pattern is shown in the UV-vis absorption spectra. Indeed, the photocatalytic activity is obviously improved after the addition of these three catalysts. Photocatalytic degradation capabilities of $CsPbCl_3$ and $CsPbBr_3$ were studied, and the results indicated that 90% and 89% of MO was degraded within 100 min, respectively. Initially, the degradation efficiency of MO was higher, but it gradually slowed down as the equilibrium approached.

To further assess the photocatalytic activity, we compared the degradation ability of the $CsPbCl_3$ and $CsPbBr_3$ QDs with those of other perovskites and semiconductor nanomaterials

Table 1 Degradation rates of MO under the action of different catalysts for the same reaction time of 80 min

Sample	Morphology	Dye degradation (%)	Ref.
$CsPbCl_3$	QDs	90	This work
$CsPbBr_3$	QDs	82	This work
N-Doped $NaTaO_3$	Cubic	40	31
ZnO	Nanosheet	88	32
	Nanoflake	85	33
TiO_2 (P25)	Nanoparticle	80	34

(Table 1). Compared to other catalysts, $CsPbCl_3$ QDs do have better photocatalytic performance.

In addition, the photocatalytic reaction is mainly due to the arrangement of surface atoms and the contact surface between the catalyst and organic pollutants.[35] The optimum content of $CsPbCl_3$ and $CsPbBr_3$ is an important factor that affects the photodegradation of MO. To optimize the catalyst dose, photocatalytic experiments were performed by varying the contents of the catalyst from 0.1 mg to 3 mg. Fig. 3c and S4a† show the change in the concentrations of MO with different amounts of catalyst. The results of the experiment reveal that the degradation efficiency of MO shows a quick increase with the increasing dose of the catalyst, especially when the catalyst content is within the range of 0.1–2 mg ($CsPbCl_3$) or 0.1–1 mg ($CsPbBr_3$). This phenomenon can be explained in terms of the active sites on the catalyst surface, the penetration of light into the solution, and the contact area of the dye and the catalyst.[31] An increase in the content of catalysts increases the amount of active sites, which in turn increases the number of hydroxyl ($^{\bullet}OH$) and superoxide ($^{\bullet}O_2^-$) radicals. Therefore, the degradation efficiency improves with the increase in the catalyst dose. However, the degradation efficiency is reduced when the content of the catalyst exceeds the abovementioned range. This observation can be accounted for the agglomeration of the catalyst with the increasing content; this in turn reduces the penetration of light as well as the contact of the dye and the catalyst. Thus, as the catalyst dose exceeds the optimum content, the degradation efficiency is reduced. The order of the photocatalytic performance of $CsPbBr_3$ is $CsPbBr_3$-1 mg > $CsPbBr_3$-0.5 mg > $CsPbBr_3$-1.5 mg > $CsPbBr_3$-0.1 mg. In addition, the order of the photocatalytic performance of $CsPbCl_3$ is $CsPbCl_3$-2 mg > $CsPbCl_3$-1 mg > $CsPbCl_3$-3 mg > $CsPbCl_3$-0.1 mg. Therefore, the optimum contents of $CsPbCl_3$ and $CsPbBr_3$ are $CsPbCl_3$-2 mg and $CsPbBr_3$-1 mg, respectively. Moreover, compared to $CsPbBr_3$ QDs, $CsPbCl_3$ QDs demonstrate more excellent photocatalytic performance; this is because the small particle size of the $CsPbCl_3$ QDs can offer large interfacial surface areas and short electron–hole diffusion lengths to the internal interfaces.

To eliminate the high surface area effects of $CsPbCl_3$ as compared to those of the large-sized $CsPbBr_3$, a series of contrast tests was conducted by increasing the mass ratio of $CsPbBr_3$ to $CsPbCl_3$. As shown in Fig. S5 and S6,† the $CsPbCl_3$-2 mg shows the best photocatalytic activity as compared to the excess $CsPbBr_3$ catalyst (4 mg, 6 mg, and 8 mg) during the whole photocatalysis process, and more than 90% of MO is decomposed by the $CsPbCl_3$-2 mg catalyst. More importantly, the $CsPbCl_3$-2 mg catalyst shows much higher photocatalytic performance (almost twofold activity) than the $CsPbBr_3$ catalyst in the first 20 minutes. Therefore, the higher photocatalytic activity of $CsPbCl_3$ can be attributed to the inherent structure and components, whereas the surface area disparity is compensated by different amounts of $CsPbBr_3$.

The change in the MO degradation efficiency ($1 - C_t/C_0$) is calculated from different MO solution absorption peaks (Fig. 3e, h, and Fig. S7†). The intersection of these two curves indicates the half-life of the MO dye, which is the time required for MO solution concentration to decrease by half.[36] For the catalysts $CsPbCl_3$-2 mg and $CsPbBr_3$-1 mg, based on the curves, the half time decreases and the photodegradation activity is enhanced.

To determine the intermediates formed during the degradation process over $CsPbBr_3$, ESI-MS was used, and mass spectrum intensity of the fragment ion peaks at different illumination times is shown in Fig. S8.† At 0 min, there is a strong peak at m/z = 304 corresponding to MO in the aqueous solution, and after visible light irradiation (20 min, 40 min, 60 min, 80 min, and 100 min) with the photocatalyst, several new peaks associated with MO degradation are observed such as m/z = 290, 276, 256, 242, 226, 157, and 80.[30] These peaks with lower mass than that of MO indicate that the structural ring is partially cracked. The peak of m/z 290 can be attributed to the loss of one methyl group from MO. The fragment ion m/z 276 corresponds to [M − Na − CH_3], m/z 226 corresponds to [M − Na − SO_2^-], m/z 157 corresponds to [M − Na − $N_2C_6H_4NH_2$], and m/z 80 corresponds to SO_3^-. Along with the prolongation of irradiation time, some degradation intermediate products first increased and then gradually decomposed to smaller fragment ions. Fig. 4 shows the proposed intermediate products of MO. It is interesting to note that the decomposition of organic dyes results in the decolorization of the solution, as shown by the ESI-MS, and the intermediates formed do not exhibit high toxicity as compared to the starting molecule.

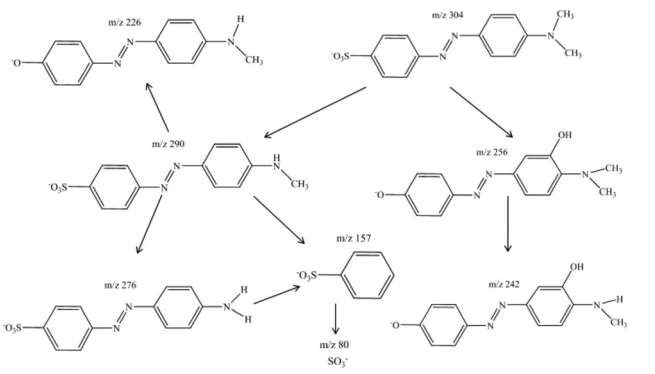

Fig. 4 The proposed degradation products of MO.

Visible light-driven photocatalytic mechanism of the $CsPbX_3$ QD catalysts

Under visible light irradiation, photogenerated $^{\bullet}O_2^-$, holes (h^+) and $^{\bullet}OH$ play an important role in the degradation of organic dyes.[37] To further understand the photocatalytic mechanism and find out which radical dominates during the photocatalytic degradation of MO, trapping experiments are conducted. Benzoquinone (BQ), ethylenediaminetetraacetic acid disodium salt (EDTA-2Na), and isopropanol (IPA) are used as radical trappers for $^{\bullet}O_2^-$, h^+, and $^{\bullet}OH$, respectively. The experimental procedure is similar to the photodegradation of MO experiments, except that 3 mL of MO solution is replaced by 3 mL of a mixture of the dye and the scavenger. (1) When BQ is used to capture $^{\bullet}O_2^-$, the absorption intensity evidently decreases with the irradiation time (Fig. 5b). (2) When EDTA-2Na is used as the h^+ scavenger (Fig. 5c), the absorption intensity slowly decreases with the irradiation time. (3) When IPA is used as the $^{\bullet}OH$ scavenger (Fig. 5d), a change occurs in the peak intensity similar to (2). The corresponding curve of the C_t/C_0 is shown in Fig. 5a. The obviously decreasing degradation rate with the addition of 0.2 mmol BQ implies that $^{\bullet}O_2^-$ plays a much more important role than h^+ and $^{\bullet}OH$ in the photodegradation process.

Based on the experimental results, the photocatalytic reaction mechanism of $CsPbX_3$ QDs can be explained as follows (Fig. 6): when $CsPbX_3$ QDs are irradiated by light with an energy higher or equal to the band gap, the absorption of photons by $CsPbX_3$ QDs leads to the excitation of e^- from the valence band (VB) to the conduction band (CB) while leaving a h^+ on the VB; after photoexcitation, there is no migration of e^- to the conduction or valence bands; mainly, before electron–hole recombination, the e^- returns to the LUMO state (on the CB), whereas the h^+ migrates to the HOMO state (on the VB). The LUMO/HOMO energy gap establishes the band-gap. In addition, since the redox potential of H_2O (OH^-)/$^{\bullet}OH$ and O_2/$^{\bullet}O_2^-$ lies within the band gap of the $CsPbX_3$ QDs, $^{\bullet}O_2^-$ can be generated by the capture of electrons in the CB. The photo-induced h^+ can be trapped to produce $^{\bullet}OH$, which are speculated to be responsible for dye degradation. The main reaction process involved in the photocatalytic degradation of MO is shown in the following equation:[31,38,39]

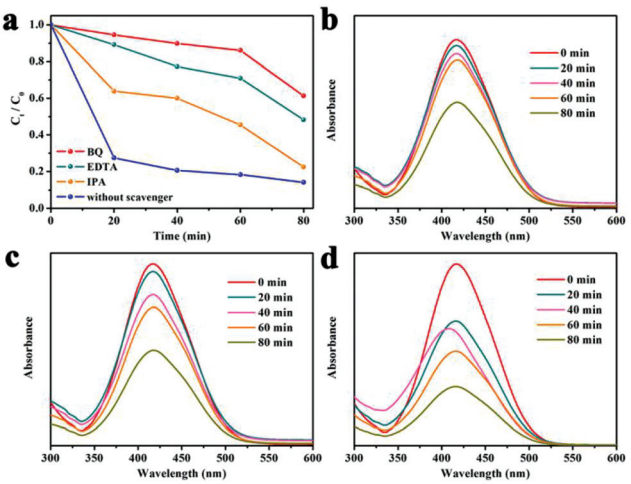

Fig. 5 (a) Concentration (C_t/C_0) changes of MO in the presence of different radical trappers. The UV-vis spectra changes of MO during the trapping experiments conducted using (b) BQ, (c) EDTA-2Na, and (d) IPA.

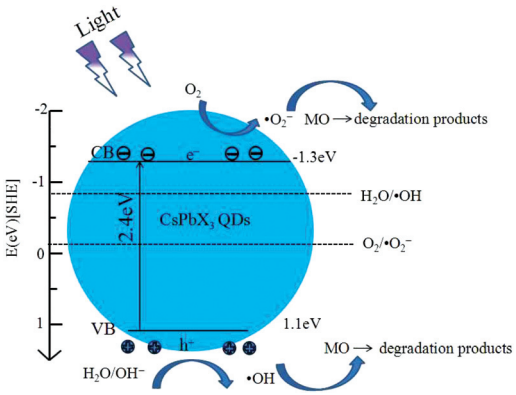

Fig. 6 Proposed mechanisms for the photocatalytic reaction of MO using $CsPbX_3$ QDs.

$$CsPbX_3\ QDs + h\nu \rightarrow e^- + h^+ \quad (1)$$

$$O_2 + e^- \rightarrow {}^{\bullet}O_2^- \quad (2)$$

$$H_2O/OH^- + h^+ \rightarrow {}^{\bullet}OH \quad (3)$$

$$Dye + {}^{\bullet}OH/{}^{\bullet}O_2^- \rightarrow intermediates \rightarrow degradation\ products \quad (4)$$

The reusability of the sample $CsPbCl_3$-2 mg is tested in the photodegradation of MO over two cycles under visible light irradiation (Fig. S9†). After the first cycle of photocatalysis experiment, the dye solution is adjusted to the initial concentration. The stability experiment demonstrates that the photocatalytic activity of $CsPbCl_3$ does not significantly change after two cycles. It obviously proves that the $CsPbCl_3$ QD photocatalyst has good stability during the photocatalytic reaction.

Conclusions

In summary, $CsPbX_3$ QDs are successfully fabricated by an emulsion fabrication and demulsion method at room temperature. The microstructure of $CsPbX_3$ QDs is investigated, and it has been observed that $CsPbX_3$ QDs show a spherical shape with a reasonable monodispersed distribution. The photocatalytic performance of $CsPbX_3$ QDs is explored for the degradation of organic dyes (for example, MO). Both $CsPbCl_3$ and $CsPbBr_3$ QDs show better photocatalytic performance, which can decompose 90% and 89% of MO within 100 min, respectively. Further experiments suggest that MO is indeed broken down into smaller fragments and relatively non-toxic substances. The trapping experiments suggest that $^{\bullet}O_2^-$ plays a

more important role than h^+ and $^{\bullet}OH$ in the photocatalytic process. These experiment results show that $CsPbX_3$ QDs are promising to be used as a high-performance visible light-driven photocatalyst and provide a new insight into the study of $CsPbX_3$ QDs, enhancement of the photocatalytic degradation efficiency, and further utilization in the field of energy transformation or environmental improvement.

Experimental

Preparation of $CsPbX_3$ QDs

All the reagents were purchased from Aladdin and used directly without purification. $CsPbX_3$ QDs were synthesized according to a previous report.[20] In the synthesis of $CsPbBr_3$, 0.4 mmol $PbBr_2$ was first added to 10 mL DMSO solution and stirred until dissolved; then, 1 mL OA and 0.5 mL OAm were added to the precursor solution to form a stable environment. Then, 0.4 mmol CsBr was added. After a period of stirring, 1 mL of the precursor solution was rapidly added to 10 mL toluene under vigorous stirring. Other samples were fabricated with the mixture of PbX_2 and CsX (X = Cl, Br, and I). All experiments were carried out at room temperature.

Purification of $CsPbX_3$ QDs

The purification procedures of $CsPbX_3$ QDs are as follows:[40] first, excess ethanol is added to precipitate the QDs, and the solid is obtained after centrifugation. Then, the QDs are redispersed in a mixture of toluene and ethanol. The solution is centrifuged again, and this process is repeated several times.

Characterizations and measurements

The crystallographic information of the samples was obtained by XRD with Cu Kα radiation (Rigaku, Tokyo, Japan). The scan range (2θ) was 10–70°, and the scan rate was 2° min^{-1}. The microstructure and morphology of the as-prepared samples were obtained by TEM and HRTEM. Low-resolution TEM images were obtained using the HITACHI H-600 Analytical TEM with an accelerating voltage of 100 kV. HRTEM measurements were carried out using the JEM-2100F high-resolution transmission electron microscope operating at 200 kV. The elements were analyzed by energy-dispersive X-ray spectroscopy (EDX) attached to the XL-30 SEM (Philips-FEI XL-30 EDX). The absorption spectra were obtained using a UV-vis spectrophotometer from 300 nm to 600 nm (Shimadzu UV-3101PC) at room temperature. The residual dye and intermediates of MO were analyzed by electrospray ionization mass spectrometry (ESI-MS, Quattro Premier XE Electron Spray Ionization Source).

Photocatalytic activity measurement

The photocatalytic activity of $CsPbX_3$ QDs was evaluated *via* the decomposition of MO under visible light irradiation. A 500W Xe light was used as a light source and kept 15 cm away from the photocatalytic reactor. Typically, the as-obtained $CsPbX_3$ QDs were added to 3 mL of MO solution (10 mg L^{-1}). The suspension was ultrasonicated for 5 min to make the catalyst and MO solution react completely. Then, the suspension was placed in the dark for 30 min to reach the adsorption–desorption equilibrium between MO and the photocatalyst. After this, the suspension was exposed to light irradiation for photocatalytic activity measurement, and the photocatalyst powders were separated through centrifugation. The absorption spectrum of the MO solution was tested by a UV-vis spectrophotometer in the range from 300 nm to 600 nm.

Acknowledgements

This work was supported by the National Nature Science Foundation of China (no. 61504145) and Science and Technology Planning Project of Guangdong Province (no. 2016B020240006 and No. 2014B01008016).

Notes and references

1 A. Kudo and Y. Miseki, *Chem. Soc. Rev.*, 2009, **38**, 253–278.
2 M. G. Walter, E. L. Warren, J. R. McKone, S. W. Boettcher, Q. Mi, E. A. Santori and N. S. Lewis, *Chem. Rev.*, 2010, **110**, 6446–6473.
3 X. Chen and S. S. Mao, *Chem. Rev.*, 2007, **107**, 2891–2959.
4 X. Lang, W. Ma, C. Chen, H. Ji and J. Zhao, *Acc. Chem. Res.*, 2014, **47**, 355–363.
5 S. Sadhishkumar and T. Balusamy, *Renewable Sustainable Energy Rev.*, 2014, **37**, 191–198.
6 G. Chen, J. Seo, C. Yang and P. N. Prasad, *Chem. Soc. Rev.*, 2013, **42**, 8304–8338.
7 M. Kitano and M. Hara, *J. Mater. Chem.*, 2010, **20**, 627–641.
8 M. N. Chong, B. Jin, C. W. K. Chow and C. Saint, *Water Res.*, 2010, **44**, 2997–3027.
9 V. Siva Reddy, S. C. Kaushik, K. R. Ranjan and S. K. Tyagi, *Renewable Sustainable Energy Rev.*, 2013, **27**, 258–273.
10 Z. Li, W. Luo, M. Zhang, J. Feng and Z. Zou, *Energy Environ. Sci.*, 2013, **6**, 347–370.
11 T. Kawai and T. Sakata, *Nature*, 1979, **282**, 283–284.
12 L. Xu, Y. L. Hu, C. Pelligra, C. H. Chen, L. Jin, H. Huang, S. Sithambaram, M. Aindow, R. Joesten and S. L. Suib, *Chem. Mater.*, 2009, **21**, 2875–2885.
13 L. L. Zhu, M. H. Hong and G. W. Ho, *Sci. Rep.*, 2015, **5**, 11609.
14 P. Kundu, P. A. Deshpande, G. Madras and N. Ravishankar, *J. Mater. Chem.*, 2011, **21**, 4209–4216.
15 G. Gao, Q. Xi, H. Zhou, Y. Zhao, C. Wu, L. Wang, P. Guo and J. Xu, *Phys. Chem. Chem. Phys.*, 2017, **19**, 11366–11372.
16 G. Zhang, G. Liu, L. Wang and J. T. S. Irvine, *Chem. Soc. Rev.*, 2016, **45**, 5951–5984.
17 L. Protesescu, S. Yakunin, M. I. Bodnarchuk, F. Krieg, R. Caputo, C. H. Hendon, R. X. Yang, A. Walsh and M. V. Kovalenko, *Nano Lett.*, 2015, **15**, 3692–3696.

18 J. Song, J. Li, X. Li, L. Xu, Y. Dong and H. Zeng, *Adv. Mater.*, 2015, **27**, 7162–7167.
19 Y. Wang, X. Li, J. Song, L. Xiao, H. Zeng and H. Sun, *Adv. Mater.*, 2015, **27**, 7101–7108.
20 X. Li, Y. Wu, S. Zhang, B. Cai, Y. Gu, J. Song and H. Zeng, *Adv. Funct. Mater.*, 2016, **26**, 2435–2445.
21 L. E. Brus, *J. Chem. Phys.*, 1984, **80**, 4403–4409.
22 D. V. Talapin, J. S. Lee, M. V. Kovalenko and E. V. Shevchenko, *Chem. Rev.*, 2010, **110**, 389–458.
23 A. J. Nozik, M. C. Beard, J. M. Luther, M. Law, R. J. Ellingson and J. C. Johnson, *Chem. Rev.*, 2010, **110**, 6873–6890.
24 Y. Shirasaki, G. J. Supran, M. G. Bawendi and V. Bulović, *Nat. Photonics*, 2012, **7**, 13–23.
25 X. Zhang, B. Xu, J. Zhang, Y. Gao, Y. Zheng, K. Wang and X. Sun, *Adv. Funct. Mater.*, 2016, **26**, 4595–4600.
26 A. Swarnkar, A. R. Marshall, E. M. Sanehira, B. D. Chernomordik, D. T. Moore, J. A. Christians, T. Chakrabarti and J. M. Luther, *Science*, 2016, **354**, 92–95.
27 M. A. Malik, M. Y. Wani and M. A. Hashim, *Arabian J. Chem.*, 2012, **5**, 397–417.
28 W. L. Ong, M. Gao and G. W. Ho, *Nanoscale*, 2013, **5**, 11283–11290.
29 W. L. Ong, S. Natarajan, B. Kloostra and G. W. Ho, *Nanoscale*, 2013, **5**, 5568–5575.
30 T. Chen, Y. Zheng, J. Lin and G. Chen, *J. Am. Soc. Mass Spectrom.*, 2008, **19**, 997–1003.
31 D. R. Liu, Y. S. Jiang and G. M. Gao, *Chemosphere*, 2011, **83**, 1546–1552.
32 F. Xu, Y. Shen, L. Sun, H. Zeng and Y. Lu, *Nanoscale*, 2011, **3**, 5020–5025.
33 Y. Li, H. F. Zuo, Y. R. Guo, T. T. Miao and Q. J. Pan, *Nanoscale Res. Lett.*, 2016, **11**, 260.
34 W. Li, D. Li, Y. Lin, P. Wang, W. Chen, X. Fu and Y. Shao, *J. Phys. Chem. C*, 2012, **116**, 3552–3560.
35 S. H. M. Navaneethan, J. Archana, A. Silambarasan, S. Ponnusamy, C. Muthamizhchelvan and Y. Hayakawa, *Dalton Trans.*, 2015, **44**, 10490–10498.
36 A. A. P. Mansur, H. S. Mansur, F. P. Ramanery, L. C. Oliveira and P. P. Souza, *Appl. Catal., B*, 2014, **158–159**, 269–279.
37 B. Tian, R. Dong, J. Zhang, S. Bao, F. Yang and J. Zhang, *Appl. Catal., B*, 2014, **158–159**, 76–84.
38 M. Sun, D. Li, W. Zhang, Z. Chen, H. Huang, W. Li, Y. He and X. Fu, *J. Phys. Chem. C*, 2009, **113**, 14916–14921.
39 C. W. Yen, M. A. Mahmoud and M. A. El-Sayed, *J. Phys. Chem. A*, 2009, **113**, 4340–4345.
40 X. Li, D. Yu, F. Cao, Y. Gu, Y. Wei, Y. Wu, J. Song and H. Zeng, *Adv. Funct. Mater.*, 2016, **26**, 5903–5912.